

# Neglecting Primordial non-Gaussianity Threatens Future Cosmological Experiment Accuracy

Stefano Camera,<sup>1,2,\*</sup> Carmelita Carbone,<sup>3,4</sup> Cosimo Fedeli,<sup>5</sup> and Lauro Moscardini<sup>6,5,4</sup>

<sup>1</sup>*Jodrell Bank Centre for Astrophysics, School of Physics and Astronomy,  
The University of Manchester, Oxford Road, Manchester M13 9PL, UK*

<sup>2</sup>*CENTRA, Instituto Superior Técnico, Universidade de Lisboa,  
Avenida Rovisco Pais 1, 1049-001 Lisboa, Portugal*

<sup>3</sup>*INAF, Osservatorio Astronomico di Brera, Via Bianchi 46, 23807 Merate (LC), Italy*

<sup>4</sup>*INFN, Sezione di Bologna, Viale Berti Pichat 6/2, 40127 Bologna, Italy*

<sup>5</sup>*INAF, Osservatorio Astronomico di Bologna, Via Ranzani 1, 40127 Bologna, Italy*

<sup>6</sup>*Dipartimento di Fisica e Astronomia, Alma Mater Studiorum  
Università di Bologna, Viale Berti Pichat 6/2, 40127 Bologna, Italy*

(Dated: Received July 26, 2018; published – 00, 0000)

Future galaxy redshift surveys aim at probing the clustering of the cosmic large-scale structure with unprecedented accuracy, thus complementing cosmic microwave background experiments in the quest to deliver the most precise and accurate picture ever of our Universe. Analyses of such measurements are usually performed within the context of the so-called vanilla  $\Lambda$ CDM model—the six-parameter phenomenological model which, for instance, emerges from best fits against the recent data obtained by the Planck satellite. Here, we show that such an approach is prone to subtle systematics when the Gaussianity of primordial fluctuations is concerned. In particular, we demonstrate that, if we neglect even a tiny amount of primordial non-Gaussianity—fully consistent with current limits—we shall introduce spurious biases in the reconstruction of cosmological parameters. This is a serious issue that must be properly accounted for in view of accurate (as well as precise) cosmology.

## I. INTRODUCTION

The currently accepted standard model for the formation of the cosmic structure posits that the Universe underwent an early phase of accelerated expansion [dubbed ‘inflation’, 1] during which a random field of primordial density fluctuations was originated. Subsequent gravity-driven hierarchical growth of such density fluctuations led to the formation of galaxies, galaxy clusters and the cosmic large-scale structure (LSS). As inflation is not a fundamental theory, different classes of inflationary models predict different statistical distributions for the primordial density fluctuations [see e.g. 2, for a comprehensive review]. Naturally, structures accreting from different initial conditions will have different statistical properties. The study of such properties constitutes one of the most powerful probes for understanding the physics of the (mostly unobservable) early Universe.

One of the most general ways to quantify the statistics of primordial density fluctuations is measuring their level of non-Gaussianity. Whilst the simplest slow-roll inflationary model predicts initial conditions that are almost perfectly Gaussian, the relaxation of specific assumptions gives rise to substantial and model-dependent deviations from Gaussianity. A particularly convenient—although not unique—way to parameterise primordial non-Gaussianity (PNG) is to add a quadratic correction

to the original Gaussian Bardeen’s potential field [3, 4],

$$\Phi = \Phi_G + f_{\text{NL}} * (\Phi_G^2 - \langle \Phi_G^2 \rangle). \quad (1)$$

The quantity dubbed  $f_{\text{NL}}$ , which may be regarded as a free parameter, determines the amplitude of PNG. In the most general case,  $f_{\text{NL}}$  may depend on both time and scale, whence the  $*$  convolution symbol instead of ordinary multiplication; as is often done in the literature, for the sake of simplicity we here assume  $f_{\text{NL}}$  to be scale independent.

PNG has been studied extensively over the past decade, using both data from the cosmic microwave background (CMB) and the LSS. With respect to the latter, investigations included cluster number counts, galaxy clustering, cosmic shear, LSS topology, and others [see for example 5–11, and references therein]. Recently, analyses of *Planck* satellite data managed to severely constrain the allowed parameter space of PNG [12]. Henceforth, according to a number of studies, only future LSS experiments that will be able to provide comparable constraints on  $f_{\text{NL}}$ . For example, via galaxy redshift surveys [11, 13–15], in the radio continuum [16, 17], with newborn techniques such as neutral hydrogen intensity mapping [18] or via cross-correlation with other observables [19–21].

Given that many LSS cosmological tests keep finding levels of PNG that are consistent with zero [though usually with large error bars, e.g. 22], and the fact that confidence levels have been dramatically shrunk by *Planck* data, it is meaningful to ask if PNG could be altogether ignored without significantly affecting constraints on the other cosmological parameters. If that is the case, the

---

\* stefano.camera@manchester.ac.uk

analysis of future cosmological data will be significantly simplified. Conversely, PNG should be kept in mind in order not to bias future cosmological constraints. This is the very question we address in this work. Specifically, we investigate whether we would introduce a bias in the best-fit value of other cosmological parameters if we neglected PNG in a Universe with a small but non-vanishing value of  $f_{\text{NL}}$ . Then, we compare this possible bias with the statistical uncertainties predicted for future LSS surveys. Throughout this paper we refer to a Class IV cosmological experiment, of which the most renowned representatives are e.g. the Square Kilometre Array [SKA, 27] at radio wavelengths, and the Dark Energy Survey [DES, 23], the forthcoming European Space Agency *Euclid*<sup>1</sup> satellite [24, 25] and the Large Synoptic Survey Telescope [LSST, 26] at optical frequencies.

As a reference model, we assume a flat  $\Lambda$ CDM Universe with total matter density (in units of the critical density)  $\Omega_m = 0.315$ , baryon fraction  $\Omega_b = 0.0487$ , dark energy equation of state CPL parameters  $w_0 = -1$  and  $w_a = 0$  [28, 29], dimensionless Hubble constant  $h \equiv H_0/(100 \text{ km/s/Mpc}) = 0.673$ ; the primordial power spectrum is described by its scalar spectral index  $n_s = 0.960$  and amplitude  $A_s = 2.195 \times 10^{-9}$  [30]. We consider cosmological constraints as expected for galaxy cluster counts, clustering of galaxies and galaxy clusters, as well as their combination.

## II. METHODOLOGY

### A. Modelling PNG Corrections

The impact of deviations from Gaussianity on the abundance and clustering of the tracers of the underlying dark matter structure have been investigated by many authors obtaining either theoretical, semi-analytic or fully numerical results. Here, we summarise the most relevant aspects and refer the interested reader to e.g. Fedeli *et al.* [11] and references therein for additional details. PNG effects mainly concern the mass function and linear bias of dark matter haloes. These modifications involve different integrals of the gravitational potential bispectrum,  $B^\Phi(\mathbf{k}_1, \mathbf{k}_2, \mathbf{k}_3)$ . The bispectrum amplitude depends on both the amplitude  $A_s$  of the gravitational potential power spectrum,  $P^\Phi(\mathbf{k})$ , and on  $f_{\text{NL}}$  so that

$$B^\Phi(\mathbf{k}_1, \mathbf{k}_2, \mathbf{k}_3) = f_{\text{NL}} A_s^2 \Gamma(\mathbf{k}_1, \mathbf{k}_2, \mathbf{k}_3). \quad (2)$$

The PNG shape is determined by the dependence of  $\Gamma(\mathbf{k}_1, \mathbf{k}_2, \mathbf{k}_3)$  upon the three momenta.

Here, we investigate the effect of some bispectrum shapes. Besides the most used local-type PNG—whose

bispectrum is maximised for squeezed configurations, where one of the three momenta is much smaller than the other two—we also consider ‘orthogonal’ PNG, so called because its configuration is nearly orthogonal to the local and equilateral shapes [see 31, for a review]. The former is known to have the heaviest impact on the clustering of the LSS, whilst the latter is nonetheless interesting because presents degeneracies with other cosmological parameters which are different to those of all other PNG types.

There are a number of prescriptions in the literature for computing PNG deviations to the abundance of dark matter haloes. Here, we follow LoVerde *et al.* [32], who used an Edgeworth expansion of the mass density field in order to derive a non-Gaussian generalisation of the Press and Schechter [33] mass function,  $n_{\text{PS}}(m, z)$ . We define a correction factor

$$\mathcal{R}(m, z) = \frac{n_{\text{PS}}(m, z)}{n_{\text{PS}}^{(\text{G})}(m, z)} \quad (3)$$

by means of which one can translate any given Gaussian halo mass function  $n^{(\text{G})}(m, z)$ , computed according to one’s favourite recipe, to its non-Gaussian counterpart, i.e.

$$n(m, z) = \mathcal{R}(m, z) n^{(\text{G})}(m, z). \quad (4)$$

In this work, we use a Gaussian Sheth and Tormen [34] mass function.

Moreover, if the initial conditions for structure formation are non-Gaussian, the linear halo bias acquires an additional scale dependence, which can be modelled as [35]

$$b(m, z, k) = b^{(\text{G})}(m, z) + \beta_R(k) \sigma_m^2 [b^{(\text{G})}(m, z) - 1]^2, \quad (5)$$

where  $b^{(\text{G})}$  is the Gaussian linear halo bias of Sheth *et al.* [36]. The function  $\beta_R(k)$  encodes all the scale dependence of the non-Gaussian halo bias at mass  $m = m(R)$ , and can be written as [37]

$$\beta_R(k) = \int_0^{+\infty} d\xi \frac{\xi^2 \mathcal{M}_R(\xi)}{8\pi^2 \sigma_m^2 \mathcal{M}_R(k)} \times \int_{-1}^1 d\cos\theta \frac{B^\Phi(\xi, \alpha, k)}{P^\Phi(k)} \mathcal{M}_R(\alpha), \quad (6)$$

with  $\alpha = \mathbf{k} + \xi$ ,  $\theta$  the angle between  $\mathbf{k}$  and  $\xi$ ,  $\sigma_m^2$  the mass variance and

$$\mathcal{M}_R(\mathbf{k}) = \frac{2T(k)W_R(k)k^2}{3H_0^2\Omega_m} \quad (7)$$

relating the density fluctuation field smoothed on a scale  $R$  to the respective peculiar potential.  $T(k)$  is the matter transfer function and  $W_R(k)$  is the Fourier transform of a top-hat window function. In the case of local bispectrum shape, it has been shown that the PNG scale dependence is  $\beta_R(k) \propto k^{-2}$  at large scales. For other shapes, the dependence is usually weaker [see 11, 13, for details].

<sup>1</sup> <http://euclid-ec.org/>

In order to model the impact of PNG and other cosmological parameters on the assembly of the LSS, we make use of the well-established halo model [38, 39]. It is a semi-analytic framework based on the fundamental assumption that all the objects we are interested in are contained within bound dark matter haloes, so that their clustering properties can be simply expressed as a superposition of the object distribution within individual haloes and the mutual clustering properties of haloes. In this framework, galaxies are distributed within dark matter haloes according to some conditional probability distribution,  $p(N_g|m)$ . (Note that in general this probability distribution would depend also on redshift, whereas for simplicity we ignore this dependence, unless explicitly stated.) Its first and second statistical moments,  $\langle N_g|m \rangle$  and  $\langle N_g(N_g - 1)|m \rangle$ , respectively represent the average number of galaxies that reside within a dark matter halo of mass  $m$  and the variance of that average number. A similar reasoning applies to clusters, except that it is commonly assumed that only one cluster may occupy a given dark matter halo, so that

$$\langle N_c(N_c - 1)|m \rangle = 0, \quad (8)$$

$$\langle N_c|m \rangle = \Theta(m - m_c), \quad (9)$$

where  $\Theta(x)$  is the Heaviside step function and  $m_c$  is some—possibly redshift-dependent—mass threshold.

Hereafter, we follow Fedeli *et al.* [11, Sec. 4] and by means of the halo model and of the quantities introduced above we consistently construct three-dimensional power spectra  $P^{XY}(k, z)$ , where  $X, Y = g, c$  for galaxies and galaxy clusters, respectively. Note that, thanks to this method, we also compute the cross-correlation power spectrum between galaxies and galaxy clusters. Eventually, we calculate number counts of galaxy clusters,  $N_c(z)$  as well.

Regarding the sources, we consider H $\alpha$  galaxies, which for instance will be selected by a *Euclid*-like experiment. These are going preferentially to be blue star-forming galaxies, therefore we model the moments of the galaxy distribution within dark matter haloes following semi-analytic models of galaxy formation [39], which give

$$\langle N_g|m \rangle = N_{g,0} \Theta(m - m_0) \left( \frac{m}{m_1} \right)^\gamma, \quad (10)$$

where  $N_{g,0} = 0.7$ ,  $m_0 = 10^{11} h^{-1} M_\odot$ ,  $m_1 = 4 \times 10^{12} h^{-1} M_\odot$ , and  $\gamma = 0.8 \Theta(m - m_0)$ . Fedeli *et al.* [11] showed that these choices of parameters produce an effective galaxy bias that is in fair agreement with predictions based on semi-analytic galaxy formation models [40, 41] for a Class IV survey like *Euclid* [42]. Moreover, we set

$$\langle N_g(N_g - 1)|m \rangle = \langle N_g|m \rangle^2 f(m), \quad (11)$$

where the function  $f(m)$  represents the deviation of the galaxy distribution from a Poissonian, and can be modelled as

$$f(m) = \begin{cases} \log^2 \sqrt{\frac{m}{m_0}} & \text{if } m \leq 10^{13} h^{-1} M_\odot \\ 1 & \text{if } m > 10^{13} h^{-1} M_\odot \end{cases}. \quad (12)$$

Finally, we consider galaxy clusters that will be photometrically selected, and for this reason we choose the minimum cluster halo mass  $m_c = m_c(z)$  using the *Euclid* Red Book photometric selection function [24].

### III. RESULTS

#### A. PNG Effects on Galaxies and Galaxy Clusters

Fig. 1 illustrates the auto- and cross-correlation power spectra of galaxies and galaxy clusters as a function of scale at  $z = 1$  for three values of  $f_{\text{NL}}$  in the local-shape scenario. Solid curves are for  $f_{\text{NL}}^{\text{loc}} = -2.17$ . We choose this particular value because, as recently remarked by Camera *et al.* [14], in  $\Lambda$ CDM with slow-roll single-field inflation, galaxy surveys should measure  $f_{\text{NL}} \simeq -2.17$ . This happens because there is a non-linear general relativistic correction on very large scales which mimics a local PNG with  $f_{\text{NL}} \simeq -5/3$  [13, 43]. This correction is derived in the CMB convention because it is based on the primordial  $\Phi$ . It does not affect CMB measurements of PNG, but it must be added to the local PNG parameter for LSS. The translation from CMB to LSS convention (which we adopt here) sets  $f_{\text{NL}}^{\text{LSS}} \approx 1.3 f_{\text{NL}}^{\text{CMB}}$  [see e.g. 11], which eventually gives  $f_{\text{NL}} \simeq -2.17$ . The other two sets of spectra are for  $f_{\text{NL}}^{\text{loc}} = 3.51$  and  $9.3$  (short- and long-dashed curves, respectively). The former has been chosen because it is the *Planck* best-fit value (LSS convention) [12], whilst the latter better shows the PNG departure from the Gaussian prediction still lying within *Planck*  $1\sigma$  bound.

From Fig. 1 we can extract some useful information. As expected, galaxy clusters (blue curves) are more biased than galaxies (red curves), so that their power spectrum is larger. Given this, the PNG correction, which is proportional to  $[b^{(G)} - 1]^2 k^{-2}$ , kicks in at smaller scales (larger wavenumbers) compared to galaxies, as it can be seen by looking at the different behaviour of the two curves at small  $k$ . Besides, we can notice that the cross-spectrum between galaxies and galaxy clusters (magenta curve set) is not merely an average of the two progenitors' spectra. Indeed, the three spectra are characterised by different scale dependences, which means that each observable carries a different piece of information about the clustering of the LSS. For instance, the different shapes at large  $k$ , whereby the galaxy 1-halo term carrying information on non-linear scales starts to become important, but no 1-halo term is present in the cluster power spectrum (since it is commonly assumed that only one cluster is contained inside each dark matter halo).

Oppositely to what happens to the power spectra, the effect of PNG on galaxy cluster counts is tinier, since it is integrated over mass and redshift. Therefore, to give a flavour of the non-Gaussian mass function, in Fig. 2 we plot the correction factor of Eq. (3),  $\mathcal{R}(m, z)$ , at  $z = 1$  and for the same  $f_{\text{NL}}$  values as in Fig. 1.

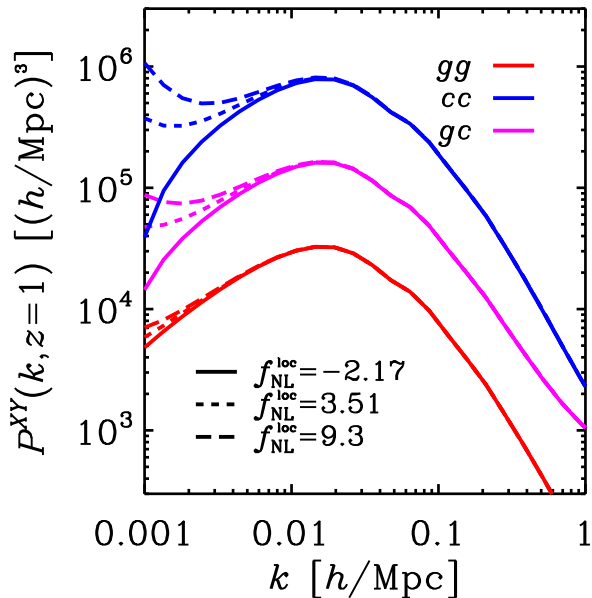


FIG. 1. Galaxy (red) and galaxy cluster (blue) power spectra and their cross-spectrum (magenta) at  $z = 1$  with  $f_{\text{NL}}^{\text{loc}} = -2.17, 3.51$  and  $9.3$  (solid, short- and long-dashed curves, respectively).

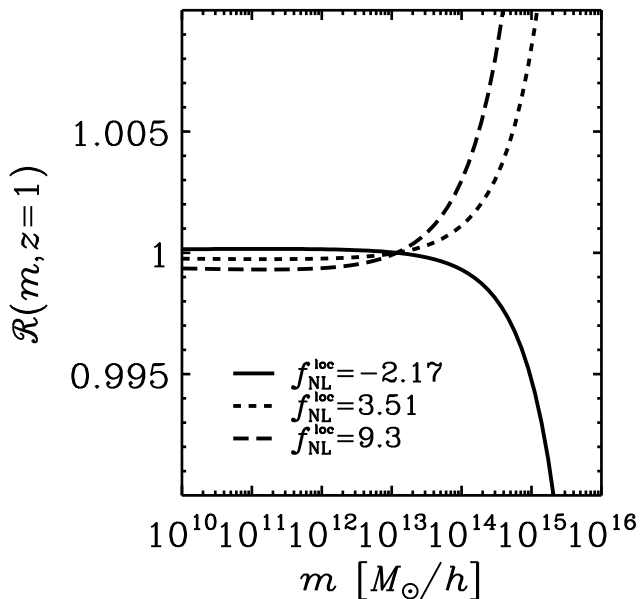


FIG. 2. Ratio of the non-Gaussian Press and Schechter mass function to the Gaussian one as a function of mass at  $z = 1$  with  $f_{\text{NL}}^{\text{loc}} = -2.17, 3.51$  and  $9.3$  (solid, short- and long-dashed curves, respectively).

## B. Induced Bias on Cosmological Parameters

To estimate the bias on a set of cosmological parameters  $\{\vartheta_\alpha\}$  triggered by neglecting some amount of PNG in the data analysis phase, we follow the Bayesian approach of Heavens *et al.* [44], based on the Fisher information matrix [45]. The basic idea is that if we try to fit against actual data a model which does not correctly include all the relevant effects—PNG in this case—the model likelihood in parameter space will have to shift its peak in order to account for the wrong assumption. In other words, the true parameter likelihood peaks at a certain point in the full parameter space spanned by  $\{\vartheta_\alpha\} \cup \{f_{\text{NL}}\}$ ; by neglecting PNG, however, we actually look at the  $f_{\text{NL}} = 0$  hypersurface, where the likelihood maximum will not in general correspond to its true value. The corresponding shift induced on the other model parameters, what we here call the bias  $b(\vartheta_\alpha)$ , is directly proportional to  $\delta f_{\text{NL}} \equiv f_{\text{NL}}^{\text{true}} - 0$  and may be computed via

$$b(\vartheta_\alpha) = -(\mathbf{F}^{-1})_{\alpha\beta} \hat{\mathbf{F}}_{\beta f_{\text{NL}}} \delta f_{\text{NL}}, \quad (13)$$

where  $\mathbf{F}_{\alpha\beta}$  is the Fisher matrix for the wrong parameter set,  $\hat{\mathbf{F}}_{\alpha\beta}$  is the true Fisher matrix for the full parameter set (including  $f_{\text{NL}}$ ) and  $\hat{\mathbf{F}}_{\beta f_{\text{NL}}}$  is a vector corresponding to the  $\hat{\mathbf{F}}$  matrix line/column relative to  $f_{\text{NL}}$ .

Details on the Fisher information matrices for galaxy and cluster power spectra and their mutual cross-spectrum can be found in Refs [11, 46]. In the following analysis, we consider 10 redshift bins of width 0.1 centred from  $z = 0.9$  to  $1.8$ . We hold  $k_{\text{max}} = 0.3h \text{ Mpc}^{-1}$  fixed to avoid the strongly non-linear régime, whilst the smallest wavenumber,  $k_{\text{min}}$ , matches the largest available scale in a given redshift bin. (To this concern, notice that general relativistic corrections on very large scales may affect the results [e.g. 14, 47], but it has been shown that for future surveys, for instance *Euclid*, their effect should be negligible [48].) Fig. 3 shows  $|b(\vartheta_\alpha)/\sigma(\vartheta_\alpha)|$  for the case where we sum the Fisher matrices for all probes, i.e. for galaxies, clusters, their cross-spectrum and cluster number counts. We present the bias in units of the forecast marginal error on the corresponding parameter,

$$\sigma(\vartheta_\alpha) = \sqrt{(\mathbf{F}^{-1})_{\alpha\alpha}}, \quad (14)$$

better to assess the impact that such a bias will imply. The parameter set which we allow to vary is the full  $\Lambda$ CDM set  $\{\vartheta_\alpha\} = \{\Omega_m, \Omega_b, w_0, w_a, h, \ln(10^{10} A_s), n_s\}$ , in addition to the PNG parameter  $f_{\text{NL}}$ . Data-points refer to sampled  $f_{\text{NL}}$  values, whereas solid curves come from the analytic expression of Eq. (13). Clearly, there are parameters prone to having their ‘best-fit’ value shifted if we estimate them within the wrong theoretical framework. This is the case of  $\Omega_m, n_s$  and  $A_s$ , known to be more degenerate with  $f_{\text{NL}}$  (see correlation coefficients in Tables I and II and related discussion). On the other hand, our analysis is in good agreement with the literature, as we



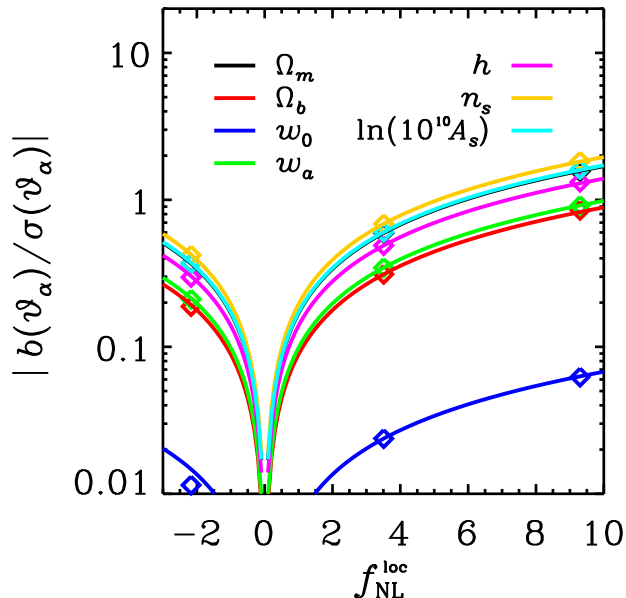


FIG. 3. Bias on cosmological parameters (in units of the error on the corresponding parameter) induced by neglecting PNG versus  $f_{\text{NL}}^{\text{loc}}$  when Fisher matrices for all probes are considered.

do not observe a significant dependence of  $\sigma(\vartheta_\alpha)$  upon the assumed  $f_{\text{NL}}$  fiducial value [see e.g. 49, 50].

Ultimately, this means that a blatant disregard for PNG (somehow understandable given the stringent *Planck* limits) may threaten future survey constraining power—if not by worsening their precision, by undermining their accuracy. Surely, a Fisher matrix approach does not fully capture the likelihood properties on the whole parameter space. Nevertheless, we want to emphasise that our analysis by no means refers to some extreme situation. On the contrary, the  $f_{\text{NL}}$  fiducial values here considered are well within *Planck*  $2\sigma$  constraints for local-type PNG.

To stress this point further on, in Fig. 4 we present  $1\sigma$  joint marginal contours in the  $[\Omega_m, \ln(10^{10} A_s)]$  and  $(w_0, w_a)$  planes (left and right panels, respectively), with solid lines for the true error contours from  $\hat{\mathbf{F}}$  and dashed contours from having neglected  $f_{\text{NL}}$  in the Fisher analysis. This is done for local-type PNG with  $f_{\text{NL}}^{\text{loc}} = 9.3$  (left plots in both panels) and for orthogonal-type PNG with  $f_{\text{NL}}^{\text{ort}} = -65$  (right plots in both panels), when we consider Fisher matrices for all probes (‘TOT’, top plots) or only for the combination of the three auto- and cross-spectra (‘PSTOT’, bottom plots). Black and red ellipses refer to forecasts either ignoring or including current *Planck* constraints. It is clear that in both cases, and for all the configurations and PNG choices considered in this work, some non-negligible shift occurs. A more quantitative insight can be drawn from Tables I and II, where relevant quantities on  $\Lambda$ CDM cosmological parameters such as forecast marginal errors  $\sigma(\vartheta_\alpha)$ ,  $f_{\text{NL}}$  correlation

parameters

$$r(\vartheta_\alpha, f_{\text{NL}}) = \frac{(\mathbf{F}^{-1})_{\alpha f_{\text{NL}}}}{\sqrt{(\mathbf{F}^{-1})_{\alpha\alpha} (\mathbf{F}^{-1})_{f_{\text{NL}} f_{\text{NL}}}}} \quad (15)$$

and normalised biases  $b(\vartheta_\alpha)/\sigma(\vartheta_\alpha)$  are given.

A major point emerging from this analysis is that, even though orthogonal-type PNG deviations from the Gaussian prediction have a much smaller impact upon the clustering of the LSS compared to PNG with local shape, current constraints on orthogonal PNG are consequently looser. In particular, *Planck* data [12] agrees with  $f_{\text{NL}}^{\text{ort}} = -33 \pm 51$  (LSS convention). That is to say, the value  $f_{\text{NL}}^{\text{ort}} = -65$  we here assume is well within *Planck*  $1\sigma$  bounds. Nonetheless, if it were the true value and we neglected it, we would miss the true likelihood peak by more than  $1\sigma$ —which is intolerable for the aims of future cosmological experiments.

#### IV. CONCLUSIONS

In this paper, we investigated the impact of neglecting PNG when performing parameter reconstruction for an idealised representative of next generation Class IV cosmological experiments. Specifically, we considered a spectroscopic galaxy redshift survey along the lines of the European Space Agency *Euclid* satellite. This allowed us to compute galaxy and galaxy cluster three-dimensional power spectra, as well as their cross-spectrum and galaxy cluster number counts, in a fully consistent way within the halo model framework.

Hence, we estimated the bias on the reconstruction of standard  $\Lambda$ CDM cosmological parameter induced by disregarding PNG in the analysis. This has been done in a Bayesian Fisher matrix perspective, by considering the  $\Lambda$ CDM vanilla cosmological model as a subspace (in parameter space) of a  $\Lambda$ CDM Universe with PNG. In other words, we recover the concordance cosmological model if we restrict the parameter space to the  $f_{\text{NL}} = 0$  hypersurface. By doing so, the peak of the parameter likelihood on the hypersurface does not, in general, correspond to its true peak in the full parameter space—if  $f_{\text{NL}}$  is nonzero and it is not completely uncorrelated to the other cosmological parameters.

Our major results are summarised in Tables I and II and in Fig. 4. In particular, we found that an incorrect treatment of PNG in the data analysis will undermine the experimental accuracy on the reconstruction of some cosmological parameters. For example, the best-fit value of the dark energy parameters  $w_0$  will be biased by more than one standard deviation, if local-type PNG is in fact present with a value of  $f_{\text{NL}}$  consistent with  $1\sigma$  *Planck* constraints. This is mainly due to the high precision of oncoming surveys, which will provide us with very tight constraints on the  $\Lambda$ CDM model parameters. Indeed, if on the one hand their expected allowed regions in parameter space will only slightly shrink by neglecting  $f_{\text{NL}}$

TABLE I. Forecast marginal errors  $\sigma$ , correlation parameters  $r$ , and (normalised) biases on  $\Lambda$ CDM cosmological parameters  $\vartheta$  for  $f_{\text{NL}}^{\text{loc}} = 9.3$ .

Local-type PNG ( $f_{\text{NL}}^{\text{loc}} = 9.3$ )													
$\vartheta$	TOT			TOT+Planck			PSTOT			PSTOT+Planck			
	$\sigma$	$r$	$b/\sigma$	$\sigma$	$r$	$b/\sigma$	$\sigma$	$r$	$b/\sigma$	$\sigma$	$r$	$b/\sigma$	
$\Omega_m$	$1.2 \times 10^{-3}$	$5.5 \times 10^{-1}$	1.6	$9.6 \times 10^{-4}$	$4.5 \times 10^{-1}$	1.5	$1.4 \times 10^{-3}$	$6. \times 10^{-1}$	$9.6 \times 10^{-1}$	$1.2 \times 10^{-3}$	$6.7 \times 10^{-1}$	1.3	
$\Omega_b$	$8. \times 10^{-4}$	$3. \times 10^{-1}$	$8.5 \times 10^{-1}$	$2.7 \times 10^{-4}$	$-2. \times 10^{-1}$	$-6.8 \times 10^{-1}$	$8.6 \times 10^{-4}$	$2.7 \times 10^{-1}$	$4.4 \times 10^{-1}$	$2.9 \times 10^{-4}$	$-4.1 \times 10^{-1}$	$-8.1 \times 10^{-1}$	
$w_0$	$2.1 \times 10^{-2}$	$2.2 \times 10^{-2}$	$6.2 \times 10^{-2}$	$7.7 \times 10^{-3}$	$-4.3 \times 10^{-1}$	-1.4	$3. \times 10^{-2}$	$-5.4 \times 10^{-1}$	$-8.6 \times 10^{-1}$	$9.5 \times 10^{-3}$	$-6.8 \times 10^{-1}$	-1.3	
$w_a$	$1. \times 10^{-1}$	$3.2 \times 10^{-1}$	$9.2 \times 10^{-1}$	$2.2 \times 10^{-2}$	$9.6 \times 10^{-2}$	$3.2 \times 10^{-1}$	$1.3 \times 10^{-1}$	$-2.3 \times 10^{-1}$	$-3.7 \times 10^{-1}$	$2.2 \times 10^{-2}$	$-1.1 \times 10^{-2}$	$-2.2 \times 10^{-2}$	
$h$	$8.9 \times 10^{-3}$	$4.6 \times 10^{-1}$	1.3	$1.9 \times 10^{-3}$	$1.6 \times 10^{-1}$	$5.4 \times 10^{-1}$	$1. \times 10^{-2}$	$4.4 \times 10^{-1}$	$7. \times 10^{-1}$	$1.9 \times 10^{-3}$	$1.4 \times 10^{-1}$	$2.8 \times 10^{-1}$	
$\ln(10^{10} A_s)$	$2.6 \times 10^{-2}$	$-5.7 \times 10^{-1}$	-1.6	$7.9 \times 10^{-3}$	$-3.3 \times 10^{-1}$	-1.1	$3. \times 10^{-2}$	$-1.8 \times 10^{-1}$	$-2.8 \times 10^{-1}$	$8. \times 10^{-3}$	$-2.1 \times 10^{-1}$	$-4.2 \times 10^{-1}$	
$n_s$	$5.7 \times 10^{-3}$	$-6.4 \times 10^{-1}$	-1.8	$2.7 \times 10^{-3}$	$-4.7 \times 10^{-1}$	-1.6	$6.7 \times 10^{-3}$	$-6. \times 10^{-1}$	$-9.7 \times 10^{-1}$	$3.1 \times 10^{-3}$	$-6.4 \times 10^{-1}$	-1.2	

 TABLE II. Same as Table I for  $f_{\text{NL}}^{\text{ort}} = -65$ .

Orthogonal-type PNG ( $f_{\text{NL}}^{\text{ort}} = -65$ )													
$\vartheta$	TOT			TOT+Planck			PSTOT			PSTOT+Planck			
	$\sigma$	$r$	$b/\sigma$	$\sigma$	$r$	$b/\sigma$	$\sigma$	$r$	$b/\sigma$	$\sigma$	$r$	$b/\sigma$	
$\Omega_m$	$1.2 \times 10^{-3}$	$-5.6 \times 10^{-1}$	2.2	$6. \times 10^{-4}$	$-2.2 \times 10^{-1}$	1.1	$1.4 \times 10^{-3}$	$-6.3 \times 10^{-1}$	1.3	$6.4 \times 10^{-4}$	$-4.1 \times 10^{-1}$	1.1	
$\Omega_b$	$8. \times 10^{-4}$	$-2.8 \times 10^{-1}$	1.1	$2.3 \times 10^{-4}$	$-4.6 \times 10^{-2}$	$2.3 \times 10^{-1}$	$8.6 \times 10^{-4}$	$-2.8 \times 10^{-1}$	$6. \times 10^{-1}$	$2.3 \times 10^{-4}$	$3.2 \times 10^{-2}$	$-8.9 \times 10^{-2}$	
$w_0$	$2.1 \times 10^{-2}$	$1.1 \times 10^{-1}$	$-4.2 \times 10^{-1}$	$1.8 \times 10^{-2}$	$-1. \times 10^{-1}$	$5.1 \times 10^{-1}$	$2.8 \times 10^{-2}$	$-4.5 \times 10^{-1}$	$9.8 \times 10^{-1}$	$2.4 \times 10^{-2}$	$-6. \times 10^{-1}$	1.7	
$w_a$	$1. \times 10^{-1}$	$-3.8 \times 10^{-1}$	1.5	$7.2 \times 10^{-2}$	$-9.2 \times 10^{-4}$	$4.6 \times 10^{-3}$	$1.3 \times 10^{-1}$	$1.2 \times 10^{-1}$	$-2.5 \times 10^{-1}$	$9.3 \times 10^{-2}$	$5.1 \times 10^{-1}$	-1.4	
$h$	$8.9 \times 10^{-3}$	$-4.5 \times 10^{-1}$	1.8	$1.8 \times 10^{-3}$	$-2.8 \times 10^{-1}$	1.4	$1. \times 10^{-2}$	$-4.5 \times 10^{-1}$	$9.7 \times 10^{-1}$	$1.9 \times 10^{-3}$	$-3.6 \times 10^{-1}$	$9.9 \times 10^{-1}$	
$\ln(10^{10} A_s)$	$2.6 \times 10^{-2}$	$5.8 \times 10^{-1}$	-2.3	$1.1 \times 10^{-2}$	$1.4 \times 10^{-1}$	$-6.9 \times 10^{-1}$	$3.1 \times 10^{-2}$	$2.5 \times 10^{-1}$	$-5.4 \times 10^{-1}$	$1.4 \times 10^{-2}$	$-4.1 \times 10^{-1}$	1.1	
$n_s$	$5.7 \times 10^{-3}$	$6.3 \times 10^{-1}$	-2.4	$2. \times 10^{-3}$	$2.6 \times 10^{-1}$	-1.3	$6.7 \times 10^{-3}$	$6.1 \times 10^{-1}$	-1.3	$2.1 \times 10^{-3}$	$3.6 \times 10^{-1}$	$-9.9 \times 10^{-1}$	

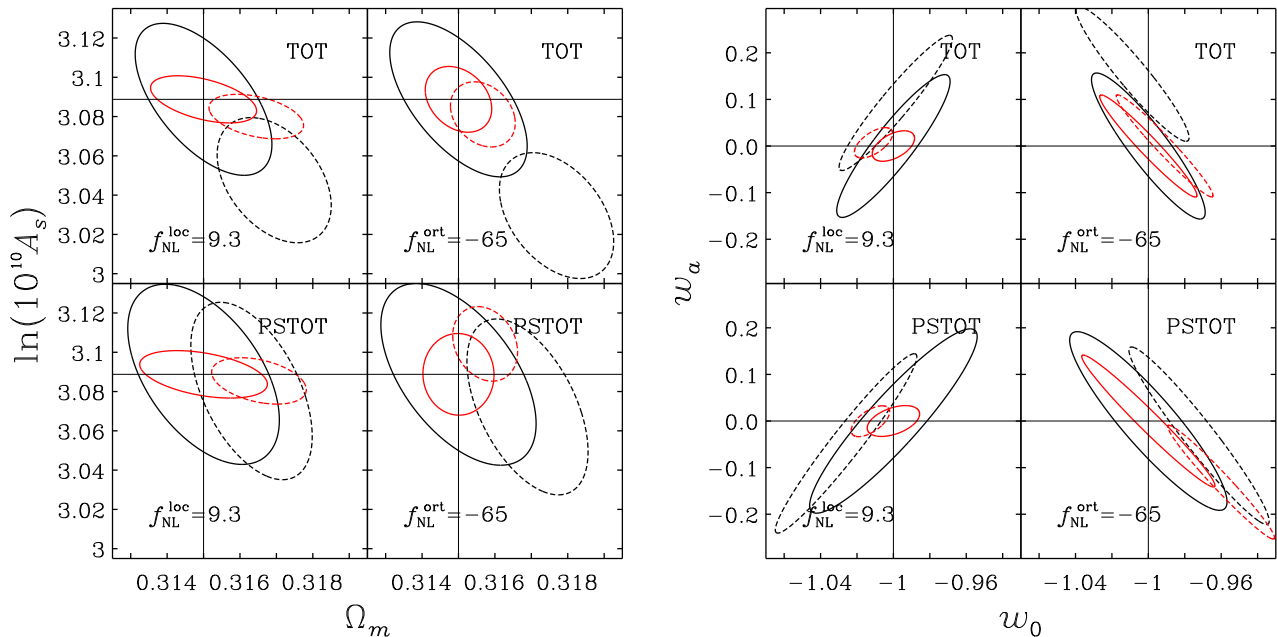


FIG. 4. Forecast  $1\sigma$  joint marginal contours in the  $[\Omega_m, \ln(10^{10} A_s)]$  and  $(w_0, w_a)$  planes (left and right panels, respectively) for local- and orthogonal-type PNG with  $f_{\text{NL}}^{\text{loc}} = 9.3$  and  $f_{\text{NL}}^{\text{ort}} = -65$ . Solid ellipses are the true error contours, whilst dashed ellipses come from neglecting  $f_{\text{NL}}$  in the analysis. Black and red colours respectively refer to results w/o and w/ *Planck* priors on  $\Lambda$ CDM parameters. Top(bottom) panels are for TOT(PSTOT).

in the analysis (as known in the literature), on the other hand the small but non-negligible degeneracy with  $f_{\text{NL}}$  will cause a shift of their reconstructed best-fit value. To avoid this, it appears clear that PNG has to be consistently accounted for.

Lastly, we emphasise that, albeit we adopt the specifics of a *Euclid*-like survey as a reference experiment, our findings should be regarded as potential systematics for the whole class of future, high-precision galaxy surveys, such as DES, LSST and the SKA.

#### ACKNOWLEDGMENTS

We thank Alan Heavens, Roy Maartens and Mario G. Santos for clarifications and comments, as well as and Ben Granett for further support. SC acknowledges support from FCT-Portugal under Post-Doctoral

Grant No. SFRH/BPD/80274/2011 and from the European Research Council under the EC FP7 Grant No. 280127. CC acknowledges financial support from the INAF Fellowships Programme 2010 and from the European Research Council through the Darklight Advanced Research Grant (No. 291521). CF has received funding from the European Commission Seventh Framework Programme (FP7/2007-2013) under grant agreement No. 267251. LM acknowledges financial contributions from contracts ASI/INAF No. I/023/12/0 ‘Attivita relative alla fase B2/C per la missione *Euclid*’, PRIN MIUR 2010-2011 ‘The dark Universe and the cosmic evolution of baryons: from current surveys to *Euclid*’, and PRIN INAF 2012 ‘The Universe in the box: multiscale simulations of cosmic structure’. SC also wishes to thank Libellulart Officina DiSegni for hospitality during the development of this work.

- 
- [1] A. H. Guth, *Phys. Rev. D* **23**, 347 (1981).
  - [2] N. Bartolo, S. Matarrese, and A. Riotto, *Phys. Rev. D* **65**, 103505 (2002).
  - [3] D. S. Salopek and J. R. Bond, *Phys. Rev. D* **42**, 3936 (1990).
  - [4] A. Gangui, F. Lucchin, S. Matarrese, and S. Mollerach, *ApJ* **430**, 447 (1994).
  - [5] S. Matarrese, L. Verde, and R. Jimenez, *ApJ* **541**, 10 (2000).
  - [6] M. Grossi, K. Dolag, E. Branchini, S. Matarrese, and L. Moscardini, *MNRAS* **382**, 1261 (2007), arXiv:0707.2516.
  - [7] C. Carbone, L. Verde, and S. Matarrese, *ApJL* **684**, L1 (2008).
  - [8] M. Grossi, L. Verde, C. Carbone, K. Dolag, E. Branchini, F. Iannuzzi, S. Matarrese, and L. Moscardini, *MNRAS* **398**, 321 (2009).

- [9] B. Sartoris, S. Borgani, C. Fedeli, S. Matarrese, L. Moscardini, *et al.*, *Mon. Not. Roy. Astron. Soc.* **407**, 2339 (2010), arXiv:1003.0841 [astro-ph.CO].
- [10] M. Maturi, C. Fedeli, and L. Moscardini, *Mon. Not. Roy. Astron. Soc.* **416**, 2527 (2011), arXiv:1101.4175 [astro-ph.CO].
- [11] C. Fedeli, C. Carbone, L. Moscardini, and A. Cimatti, *MNRAS* **414**, 1545 (2011).
- [12] P. Ade *et al.* (Planck Collaboration), *A&A* **571**, A24 (2014).
- [13] L. Verde and S. Matarrese, *ApJL* **706**, L91 (2009).
- [14] S. Camera, M. G. Santos, and R. Maartens, *ArXiv e-prints* (2014), arXiv:1409.8286.
- [15] A. Raccanelli, O. Dore, and N. Dalal, (2014), arXiv:1409.1927 [astro-ph.CO].
- [16] R. Maartens, G.-B. Zhao, D. Bacon, K. Koyama, and A. Raccanelli, *JCAP* **1302**, 044 (2013), arXiv:1206.0732 [astro-ph.CO].
- [17] L. D. Ferramacho, M. G. Santos, M. J. Jarvis, and S. Camera, *Mon. Not. Roy. Astron. Soc.* **442**, 2511 (2014), arXiv:1402.2290 [astro-ph.CO].
- [18] S. Camera, M. G. Santos, P. G. Ferreira, and L. Ferramacho, *Phys. Rev. Lett.* **111**, 171302 (2013), arXiv:1305.6928 [astro-ph.CO].
- [19] T. Giannantonio and W. J. Percival, *Mon. Not. Roy. Astron. Soc.* **441**, L16L20 (2014), arXiv:1312.5154 [astro-ph.CO].
- [20] T. Giannantonio, A. J. Ross, W. J. Percival, R. Crittenden, D. Bacher, *et al.*, *Phys. Rev.* **D89**, 023511 (2014), arXiv:1303.1349 [astro-ph.CO].
- [21] A. Raccanelli, O. Dor, D. J. Bacon, R. Maartens, M. G. Santos, *et al.*, (2014), arXiv:1406.0010 [astro-ph.CO].
- [22] S. Shandera, A. Mantz, D. Rapetti, and S. W. Allen, *JCAP* **8**, 004 (2013).
- [23] The Dark Energy Survey Collaboration, *ArXiv Astrophysics e-prints* (2005), astro-ph/0510346.
- [24] R. Laureijs *et al.* (Euclid Collaboration), *ESA-SRE* **12** (2011).
- [25] L. Amendola *et al.* (Euclid Theory Working Group), *Living Rev. Rel.* **16**, 6 (2013).
- [26] LSST Dark Energy Science Collaboration, *ArXiv e-prints* (2012), arXiv:1211.0310 [astro-ph.CO].
- [27] P. Dewdney, P. Hall, R. Schilizzi, and J. Lazio, *Proceedings of the IEEE* **97** (2009).
- [28] M. Chevallier and D. Polarski, *IJMPD* **10**, 213 (2001).
- [29] E. V. Linder, *Phys. Rev. Lett.* **90**, 091301 (2003).
- [30] P. Ade *et al.* (Planck Collaboration), *A&A* **571**, A16 (2014).
- [31] N. Bartolo, E. Komatsu, S. Matarrese, and A. Riotto, *Physics Reports* **402**, 103 (2004).
- [32] M. LoVerde, A. Miller, S. Shandera, and L. Verde, *JCAP* **4**, 14 (2008).
- [33] W. H. Press and P. Schechter, *ApJ* **187**, 425 (1974).
- [34] R. K. Sheth and G. Tormen, *MNRAS* **329**, 61 (2002).
- [35] C. Carbone, O. Mena, and L. Verde, *JCAP* **7**, 020 (2010).
- [36] R. K. Sheth, H. J. Mo, and G. Tormen, *MNRAS* **323**, 1 (2001).
- [37] S. Matarrese and L. Verde, *ApJL* **677**, L77 (2008).
- [38] U. Seljak, *MNRAS* **318**, 203 (2000).
- [39] A. Cooray and R. Sheth, *Physics Reports* **372**, 1 (2002).
- [40] C. M. Baugh, C. G. Lacey, C. S. Frenk, G. L. Granato, L. Silva, A. Bressan, A. J. Benson, and S. Cole, *MNRAS* **356**, 1191 (2005).
- [41] R. G. Bower, A. J. Benson, R. Malbon, J. C. Helly, C. S. Frenk, C. M. Baugh, S. Cole, and C. G. Lacey, *MNRAS* **370**, 645 (2006).
- [42] A. Orsi, C. M. Baugh, C. G. Lacey, A. Cimatti, Y. Wang, and G. Zamorani, *MNRAS* **405**, 1006 (2010).
- [43] M. Bruni, J. C. Hidalgo, N. Meures, and D. Wands, *Astrophys. J.* **785**, 2 (2014), arXiv:1307.1478 [astro-ph.CO].
- [44] A. F. Heavens, T. D. Kitching, and L. Verde, *MNRAS* **380**, 1029 (2007).
- [45] M. Tegmark, A. Taylor, and A. Heavens, *ApJ* **480**, 22 (1997).
- [46] G. Hütsi and O. Lahav, *A&A* **492**, 355 (2008).
- [47] S. Camera, M. G. Santos, and R. Maartens, (2014), arXiv:1412.4781 [astro-ph.CO].
- [48] J. Yoo and U. Seljak, (2013), arXiv:1308.1093 [astro-ph.CO].
- [49] E. Sefusatti, C. Vale, K. Kadota, and J. Frieman, *ApJ* **658**, 669 (2007).
- [50] T. Giannantonio, C. Porciani, J. Carron, A. Amara, and A. Pillepich, *MNRAS* **422**, 2854 (2012).